GDCh Research Article Angewandte International Edition Chemie www.angewandte.org

How to cite: *Angew. Chem. Int. Ed.* **2026**, *65*, e25369
doi.org/10.1002/anie.202525369

MOFs for Photocatalysis | Very Important Paper

Unveiling the Mechanism of Photocatalytic CO_2 Cycloaddition over Linker-Engineered Metal-Organic Frameworks

Hao Liu[+], *Yanle Li*[+], *Yunyang Qian*[+], *Yansi Tong*[+], *Qihao Yang*,* *Jungang Wang*, *Desheng Su*, *Yayun Zhao*, *Ziqi Tian*, *Zhiyi Lu*, *Hai-Long Jiang*,* *and Liang Chen**

Abstract: Photocatalytic CO_2 cycloaddition represents a promising route for solar-driven synthesis of value-added C_{2+} chemicals and simultaneously mitigating anthropogenic CO_2 emissions. However, the pivotal step of direct one-electron reduction of CO_2 to $CO_2^{\bullet-}$ requires a very high reduction potential of −1.9 V versus NHE, posing a formidable challenge. In this study, cerium-based metal-organic frameworks (MOFs) with linker-induced defects, specifically Ce-UiO-66-X (X = Me, H, and F), are investigated to elucidate the underlying mechanisms of photocatalytic CO_2 cycloaddition. Among them, Ce-UiO-66-H, which strikes an optimal balance between light absorption and charge separation, demonstrates superior catalytic performance (yield > 90%) when coupled with tetrabutylammonium bromide (TBAB) as a co-catalyst. In-situ experiments and theoretical calculations reveal that TBAB stabilizes CO_2 through the formation of $[Br^-\cdots TBA^+]\sim CO_2$ adducts, which lowers the thermodynamic energy requirement for $CO_2^{\bullet-}$ generation from 0.66 eV (in the direct CO_2-to-$CO_2^{\bullet-}$ route) to −0.90 eV. This potential modulation promotes efficient photoelectron transfer from the MOFs to CO_2, substantially enhancing the overall cycloaddition efficiency.

Introduction

Carbon capture and utilization (CCU) has emerged as a pivotal strategy for converting anthropogenic CO_2 emissions into value-added carbon feedstocks.[1–5] Among various CCU approaches, CO_2 cycloaddition with epoxides stands out for its 100% atom economy, producing multifunctional cyclic carbonates that serve as essential intermediates for high-performance plastics, non-flammable electrolyte solvents in lithium-ion batteries, fuel additives, and industrial degreasers.[6–8] Despite substantial advances in both homogeneous and heterogeneous catalysis, elevated reaction temperatures are still required to overcome the intrinsic kinetic stability of CO_2.[9–13] This energy-intensive thermal activation presents a fundamental paradox: CO_2 fixation processes dependent on fossil-derived heat inadvertently sustain carbon emissions. In this regard, leveraging solar energy as the primary activation source for CO_2 cycloaddition provides a sustainable alternative, decoupling the reaction from fossil fuel reliance and addressing the inherent contradiction of thermal-driven systems.

Significant progress has been made in developing photocatalysts such as metal oxides, metal-organic frameworks (MOFs), porous polymers, and carbon-based materials for photocatalytic CO_2 cycloaddition, aiming to promote photoexcited electron generation and directional transfer to CO_2 to form CO_2 radical anions ($CO_2^{\bullet-}$), thereby accelerating the cycloaddition process.[14–17] However, the lowest unoccupied molecular orbital (LUMO) levels of most photocatalysts fail to reach the ultra-negative potential (−1.9 V vs. NHE, pH = 7) required for CO_2-to-$CO_2^{\bullet-}$ conversion.[18–20] This intrinsic energetic mismatch challenges the prevailing assumption of direct CO_2 reduction in photocatalytic cycloaddition and necessitates a critical re-evaluation of the underlying CO_2 activation mechanism. Tetrabutylammonium bromide (TBAB) is widely employed as a co-catalyst in photocatalytic CO_2 cycloaddition due to its well-established function in thermally driven systems. While the bromide anion (Br^-) acts as a nucleophile facilitating epoxide ring-opening, the potential catalytic role of tetrabutylammonium cation

[*] H. Liu[+], Y. Tong[+], Assoc. Prof. Q. Yang, D. Su, Y. Zhao, Prof. Z. Tian, Prof. Z. Lu, Prof. L. Chen
Zhejiang Key Laboratory of Advanced Fuel Cells and Electrolyzers Technology, Ningbo Institute of Materials Technology & Engineering, Chinese Academy of Sciences, Ningbo, Zhejiang 315201, P.R. China
E-mail: yangqihao@nimte.ac.cn
chenliang@nimte.ac.cn

H. Liu[+], Assoc. Prof. Q. Yang, Prof. Z. Tian, Prof. Z. Lu, Prof. L. Chen
University of Chinese Academy of Sciences, Beijing 100049, P.R. China

Assoc. Prof. Y. Li[+]
School of Materials Engineering, Lanzhou Institute of Technology, Lanzhou, Gansu 730050, P.R. China

Dr. Y. Qian[+], Prof. H.-L. Jiang
Hefei National Research Center for Physical Sciences at the Microscale, Department of Chemistry, University of Science and Technology of China, Hefei, Anhui 230026, P.R. China
E-mail: jianglab@ustc.edu.cn

Assoc. Prof. J. Wang
China State Key Laboratory of Coal Conversion, Institute of Coal Chemistry, Chinese Academy of Sciences, Taiyuan, Shanxi 030001, P.R. China

[+] These authors contributed equally to this work.

Additional supporting information can be found online in the Supporting Information section

© 2025 Wiley-VCH GmbH

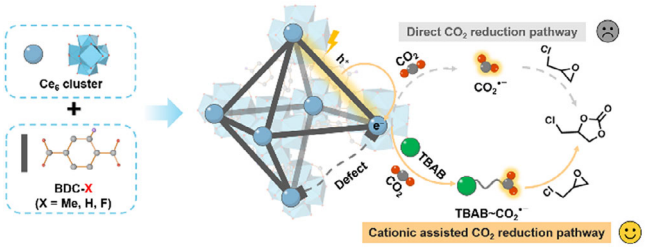

Scheme 1. Schematic illustration showing the fabrication process of Ce-UiO-66-X with controlled defect densities, revealing a cation-assisted mechanism for photocatalytic CO_2 activation in the cycloaddition reaction.

(TBA^+) has been largely overlooked.[14–16,21–23] Notably, quaternary ammonium cations analogous to TBA^+ can interact with CO_2 to form reactive adducts, substantially lowering the CO_2 reduction potential in photo- and electro-catalytic CO_2 conversion.[24–27] By analogy, a similar ammonium-assisted activation pathway may also exist in photocatalytic CO_2 cycloaddition.

MOFs, a class of porous semiconductors featuring well-defined architectures composed of inorganic metal nodes and multifunctional organic linkers,[28–36] emulate key principles of natural photosynthetic systems and provide an ideal platform for photocatalytic CO_2 conversion, particularly for mechanistic exploration.[37–42] Among them, Ce-based UiO-66 stands out as a promising candidate: the low-lying 4f orbitals of Ce^{4+} facilitate efficient linker-to-metal charge transfer (LMCT),[43–46] while its facile synthesis, exceptional structural robustness, and tunable functionality collectively enable efficient photocatalysis. Notably, the photocatalytic performance of Ce-UiO-66 is governed by two interrelated energetic parameters—ΔE_{abs} (the linker excitation energy modulated by functional groups) and ΔE_{LMCT} (the charge-transfer barrier sensitive to node defects).[43] These parameters are intrinsically coupled, such that linker modification simultaneously affects both, enabling fine-tuning of the electronic structure to achieve optimal photocatalytic efficiency.[47–50]

Herein, three isoreticular MOFs, namely Ce-UiO-66-X (X = Me, H, and F), with controlled defect densities are rationally synthesized via linker engineering. Among them, Ce-UiO-66-H exhibits an optimal balance between ΔE_{abs} and ΔE_{LMCT}, achieving >90% yield of cyclic carbonates under solvent-free conditions. In-situ diffuse reflectance infrared Fourier transform spectroscopy (DRIFTS) and electron paramagnetic resonance (EPR) spectroscopy confirm the exclusive formation of $CO_2^{\bullet-}$ species within the Ce-UiO-66-H/TBAB hybrid system, with no corresponding signals detected for a single component. In-situ EPR spectroscopy further reveals that photogenerated electrons in Ce-MOFs are transferred to CO_2 through a TBAB-assisted pathway, leading to the generation of $CO_2^{\bullet-}$ radicals (Scheme 1). Density functional theory (DFT) calculations corroborate that TBAB-assisted ($[Br^-\cdots TBA^+]\sim CO_2$) formation substantially lowers the thermodynamic energy requirement for $CO_2^{\bullet-}$ formation to −0.90 eV, compared with 0.66 eV

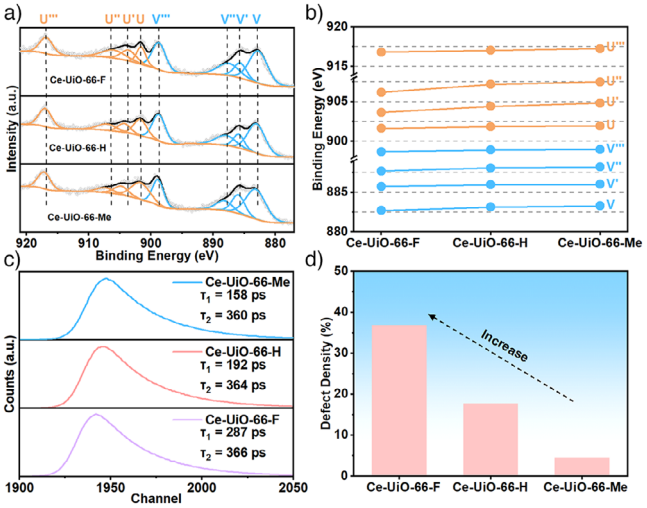

Figure 1. a) High-resolution XPS spectra of Ce 3d in Ce-UiO-66-X samples. b) Summary diagram of Ce 3d binding energies in Ce-UiO-66-X samples. c) Positron lifetime spectra for Ce-UiO-66-X samples. d) The defect density of Ce-UiO-66-X samples.

for the direct CO_2 reduction route, thereby highlighting the pivotal role of TBAB in promoting radical generation. Collectively, this study provides clear mechanistic understanding of photocatalytic CO_2 cycloaddition and unveils the previously underappreciated function of ammonium cations in modulating CO_2 activation energetics.

Results and Discussion

Synthesis and Characterization of Ce-UiO-66-X

Three isoreticular Ce-UiO-66-X (X = Me, H, and F) were synthesized via a solvothermal technique using $Ce(NH_4)_2(NO_3)_6$ and terephthalic acid derivatives (BDC-X) in a mixed solvent of N,N-dimethylformamide (DMF) and H_2O at 100 °C. Scanning electron microscopy (SEM) shows that all Ce-UiO-66-X samples exhibit uniform octahedral morphologies (Figure S1). Consistently, powder X-ray diffraction (XRD) patterns of the obtained materials coincide with the simulated UiO-66, confirming the formation of isoreticular skeletons with identical crystalline phases (Figure S2).

The established positive relationship between defect density and the Ce^{3+}/Ce^{4+} ratio in Ce-MOFs validates that X-ray photoelectron spectroscopy (XPS) as a reliable method for determining defect densities in Ce-UiO-66-X.[47] The Ce 3d spectra can be deconvoluted into eight peaks, where V and U correspond to the spin-orbit components of Ce $3d_{5/2}$ and Ce $3d_{3/2}$, respectively (Figure 1a).[51] Among the samples, Ce-UiO-66-F exhibits the lowest Ce 3d binding energy, indicative of the highest defect density, whereas Ce-UiO-66-Me shows the lowest defect concentration (Figure 1b). Positron annihilation lifetime spectroscopy (PALS) provides a powerful approach for probing structural defects in MOFs, owing to the exceptional sensitivity of positrons to atomic-scale vacancies.[52,53] PALS resolves three lifetime components (τ_1,

© 2025 Wiley-VCH GmbH

15213773, 2026, 7, Downloaded from https://onlinelibrary.wiley.com/doi/10.1002/anie.202525369 by University Of Science, Wiley Online Library on [23/02/2026]. See the Terms and Conditions (https://onlinelibrary.wiley.com/terms-and-conditions) on Wiley Online Library for rules of use; OA articles are governed by the applicable Creative Commons License

τ_2, and τ_3) with corresponding intensities (I_1, I_2, and I_3) in Ce-UiO-66-X (Figure 1c and Table S1). The longest-lived τ_3 component, associated with positron annihilation at external surfaces or interparticle voids, exhibits negligible intensity (< 1%), indicating minimal contribution from these regions. Compared to the similar τ_2 component (assigned to missing-node induced large-defect vacancies), the defect-sensitive τ_1 component, attributed to missing-linker induced Ce^{3+}-oxygen vacancies in Ce-oxo nodes,[53] shows prolonged lifetimes and elevated intensities following the order of Ce-UiO-66-F (287 ps, 24.9%) > Ce-UiO-66-H (192 ps, 11.3%) > Ce-UiO-66-Me (158 ps, 4.7%). This trend confirms that electron-withdrawing linkers facilitate defect formation, consistent with the XPS analysis. Furthermore, the increased defect density intrinsically improves framework porosity, leading to higher surface areas and pore volumes.[54–56] N_2 sorption experiments support that Ce-UiO-66-F possesses the highest BET surface area (813 $m^2 \cdot g^{-1}$) and pore volume (0.41 $cm^3 \cdot g^{-1}$), corroborating its highest defect concentration (Figure S3 and Table S2).

The missing-linker defect densities of the three Ce-UiO-66-X samples are quantified by determining the molar ratio of Ce-oxo nodes to BDC-X linkers via the dissolution-quantification coupled method, corroborated by nuclear magnetic resonance (NMR) and inductively coupled plasma mass spectrometry (ICP-MS).[48,57,58] As illustrated in Figure S4 and Table S3, the Ce-to-BDC-X molar ratios for Ce-UiO-66-Me, Ce-UiO-66-H, and Ce-UiO-66-F are 6:5.73, 6:4.94, and 6:3.78, respectively. Relative to the ideal stoichiometry of the perfect Ce-UiO-66 ($Ce_6(OH)_4O_4(BDC\text{-}X)_6$), the defect densities of three Ce-UiO-66-X MOFs are determined to be 4.5%, 17.7%, and 37.0%, respectively (Figure 1d). The thermogravimetric analysis (TGA) is also adopted to assess the defect density for the three Ce-MOF samples. The initial mass loss below 100 °C is assigned to the desorption of physisorbed water, followed minor mass loss due to μ-OH decomposition (100–200 °C). The major weight decrease above ~200 °C arises from linker combustion, ultimately yielding CeO_2 as the final residue (Figure S5 and Table S4).[58,59] The TGA-based BDC-X/Ce molar ratios for Ce-UiO-66-Me (6:5.97), Ce-UiO-66-H (6:5.03), and Ce-UiO-66-F (6:4.2) are in excellent agreement with the NMR and ICP-MS results. These results establish a clear hierarchy of defect densities, following the order Ce-UiO-66-F > Ce-UiO-66-H > Ce-UiO-66-Me, confirming the effectiveness of linker substituent-controlled defect engineering.

The Photocatalytic Performance of Ce-UiO-66-X

To evaluate the photocatalytic performance of Ce-UiO-66-X in CO_2 cycloaddition, epichlorohydrin, a representative commercial epoxide, is used as the model substrate. Under solvent-free conditions and full-spectrum irradiation, Ce-UiO-66-H exhibits the highest catalytic efficiency, affording a 92% yield of cyclic carbonate with ~100% selectivity (Figure 2a and Figure S6), surpassing Ce-UiO-66-Me (75%) and Ce-UiO-66-F (53%). Ce-UiO-66-H exhibits excellent recyclability over five consecutive cycles with preserved crystallinity and morphology (Figures S7–S9). The stability of the catalyst is further corroborated by the essentially unchanged Fourier transform infrared (FT-IR) spectra after reaction and the absence of detectable Ce leaching in the filtrate (Figure S10 and Table S5). The hot-filtration experiment shows that the slight increase in conversion matches that of TBAB alone (Figure S11), demonstrating that no catalytically active soluble species are generated during the reaction. Encouraged by its outstanding activity, various epoxides with different substituents have been examined. All substrates demonstrate excellent compatibility, achieving > 90% yields within 1.5–4 days (Table S6). Given the first-order kinetics of the CO_2 cycloaddition reaction,[60] conversion levels below 50% are used to accurately assess intrinsic photocatalytic activity. To minimize photothermal effects and isolate the true photocatalytic contribution, the reaction temperature is maintained at ~25 °C using an external cooling system (Table S7). Notably, Ce-UiO-66-H exhibits negligible thermal activity at 25 °C, with conversion remaining at ~20% in the dark regardless of catalyst presence, and similarly low activity is observed when using the free linker or the cerium precursor alone (Table S7, entries 5–8). In addition, irradiation at the same temperature boosts the conversion to 41% (Table S7, entry 1), and monochromatic-light experiments further show that the photocatalytic activity closely follows the UV-vis diffuse reflectance spectra (UV-vis DRS) (Figure S12), collectively confirming that the activity enhancement is dominantly ascribed to photoinduction.

To investigate the origin of the volcano-type trend observed in photocatalytic activity, the key electronic

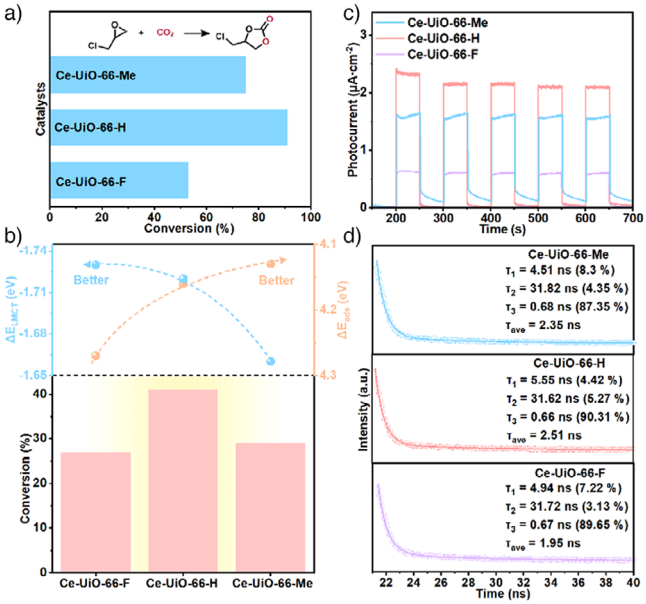

Figure 2. a) The photocatalytic performance of Ce-UiO-66-X towards CO_2 cycloaddition with epichlorohydrin, reaction condition: 20 mmol epoxides, 1 bar CO_2, 50 mg Ce-UiO-66-X, 2 mmol TBAB, 48 h, full spectrum irradiation. b) The relationship between the intrinsic activity of Ce-UiO-66-X and the calculated energy characteristics. c) Transient photocurrent response of Ce-UiO-66-X. d) Fitted time-resolved TA spectra with 320 nm laser excitation.

© 2025 Wiley-VCH GmbH

15213773, 2026, 7, Downloaded from https://onlinelibrary.wiley.com/doi/10.1002/anie.202525369 by University Of Science, Wiley Online Library on [23/02/2026]. See the Terms and Conditions (https://onlinelibrary.wiley.com/terms-and-conditions) on Wiley Online Library for rules of use; OA articles are governed by the applicable Creative Commons License

characteristics of Ce-UiO-66-X are analyzed through DFT calculations. The ΔE_{abs} follows the order of BDC-Me (4.13 eV) < BDC-H (4.16 eV) < BDC-F (4.27 eV) (Figures S13–S15). In contrast, the ΔE_{LMCT} exhibits a negative correlation with defect density. Ce-UiO-66-F possessing the highest defect density shows the lowest ΔE_{LMCT} value (−1.73 eV, Figure S15). This inverse relationship establishes a clear energetic trade-off between ΔE_{abs} and ΔE_{LMCT}, giving rise to the observed volcano-shaped activity profile (Figure 2b). Notably, Ce-UiO-66-H, with intermediate electronic properties, achieves an optimal balance between excitation energy and charge-transfer barrier, thereby delivering the highest photocatalytic efficiency among the three MOFs.

In addition, photocurrent response and time-resolved transient absorption (TA) spectroscopy are further conducted to probe the photogenerated charge carrier dynamics in Ce-UiO-66-X. In line with its superior catalytic performance, Ce-UiO-66-H exhibits the highest photocurrent density among all samples (Figure 2c), indicative of the most efficient charge separation and transfer. Further TA kinetic analyses reveal triexponential decay profiles for all three Ce-MOFs (fitting parameters in Table S8), corresponding to distinct relaxation processes. The average relaxation durations of Ce-UiO-66-F, Ce-UiO-66-Me, and Ce-UiO-66-H are 1.95, 2.35, and 2.51 ns, respectively (Figure 2d), confirming progressively enhanced excited-state persistence. All these data confirm that Ce-UiO-66-H possesses the longest-lived photogenerated charge carriers and most effectively suppresses electron-hole recombination, accounting for its optimal photocatalytic activity.

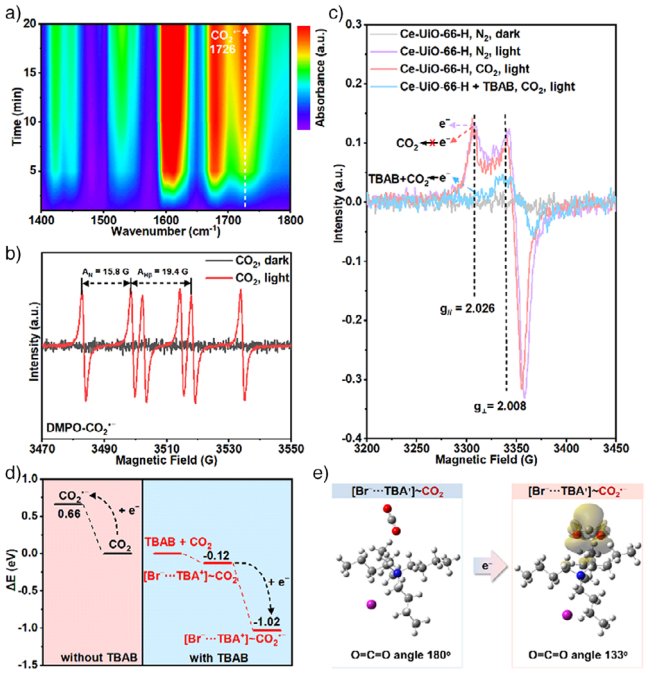

Figure 3. a) In-situ DRIFTS of the Ce-UiO-66-H and TBAB mixture with different time under light irradiation. b) EPR signals of Ce-UiO-66-H and TBAB with DMPO added under CO_2 atmosphere. c) The EPR signal of Ce-UiO-66-H at different conditions. d) Schematic diagram of electron acquisition of $[Br^-\cdots TBA^+]\sim CO_2$ complex by theoretical calculation. e) Spin density of $[Br^-\cdots TBA^+]\sim CO_2$ complex that illustrates the unpaired electron of the radical.

Mechanism of Photocatalytic CO_2 Cycloaddition

Given the potential competition between CO_2 and epoxides for the uptake of photogenerated electron-hole, experimental identification of the dominant charge transfer pathway is carried out. Mott-Schottky measurements, combined with UV–vis DRS, are used to establish the LUMO and highest occupied molecular orbital (HOMO) energy levels of Ce-UiO-66-Me, Ce-UiO-66-H, and Ce-UiO-66-F at −0.87, −0.74, and −0.79 V and 2.07, 2.22, and 2.24 V (vs. NHE, pH = 7), respectively (Figure S16,S17). The LUMO levels of Ce-MOFs (−0.7 to −0.9 V vs. NHE, pH = 7) are thermodynamically insufficient for reducing either CO_2 (−1.9 V vs. NHE, pH = 7) or epoxides (−1.5 ~ −3 V vs. NHE, pH = 7),[61,62] thereby precluding direct electron transfer to the two substrates. The possibility for epoxides oxidized by photogenerated holes is examined using 2,2,6,6-tetramethylpiperidin-1-oxyl (TEMPO) as a spin-trapping probe.[14] No discernible change in EPR signals is observed under either N_2 or CO_2 atmosphere in the Ce-UiO-66-H/epoxide system (Figure S18), indicating that photogenerated holes exert negligible oxidative influence on epoxides.

Conversely, distinct absorption bands at 1726 cm^{-1} appear in the in-situ DRIFTS spectra under light irradiation, which are indicative of the $CO_2^{\bullet-}$ species (Figure 3a).[63,64] These signals emerge exclusively in the system containing both Ce-UiO-66-H and the co-catalyst TBAB, but vanish upon removal of either component, underscoring their synergistic roles in facilitating photoinduced electron generation and transfer (Figure S19). Complementary EPR experiments employing 5,5-dimethyl-1-pyrroline N-oxide (DMPO) as a radical trapping agent provide further evidence for the formation of $CO_2^{\bullet-}$ species. The distinctive EPR signals of DMPO-$CO_2^{\bullet-}$ adducts are detected only under light irradiation in a CO_2 atmosphere containing both Ce-UiO-66-H and TBAB (Figure 3b and Figure S20). Moreover, TBAB remains structurally intact under illumination, ruling out the possibility that TBAB-derived species contribute to the detected radical signals (Figure S6). This thermodynamic limitation implies that TBAB-assisted CO_2 activation might lower the energy requirement, allowing CO_2 to more readily accept photogenerated electrons within the photocatalytic system.

In practice, TBAB serves as an indispensable component in photocatalytic CO_2 cycloaddition, where its TBA^+ cation provides a previously overlooked pathway for electron-transfer mediation. Control experiments replacing TBAB with KBr (identical anion but different cation) reveal pronounced differences. While the KBr-involved system exhibits negligible photo response and comparable yields under light and dark conditions (Table S7, entries 11–12), the TBAB-involved system displays nearly a twofold enhancement in photocatalytic conversion compared to the dark regime (Table S7, entries 1 and 7). Operando EPR spectra further elucidate the electron-transfer mechanism (Figure 3c). Ce-UiO-66-H exhibits negligible EPR signals under dark in N_2

© 2025 Wiley-VCH GmbH

15213773, 2026, 7, Downloaded from https://onlinelibrary.wiley.com/doi/10.1002/anie.202525369 by University Of Science, Wiley Online Library on [23/02/2026]. See the Terms and Conditions (https://onlinelibrary.wiley.com/terms-and-conditions) on Wiley Online Library for rules of use; OA articles are governed by the applicable Creative Commons License

atmosphere (Figure S21), whereas distinct Lorentzian signals at $g_{//} = 2.026$ and $g_{\perp} = 2.008$ emerge upon light irradiation, which can be attributed to Ce^{3+} intermediates formed in Ce-oxo nodes via the LMCT process.[65] However, these signals remain largely unchanged when N_2 is replaced with CO_2, confirming the inefficiency of direct electron transfer from Ce-MOFs to CO_2, consistent with their insufficient reduction potential for CO_2-to-$CO_2^{\bullet-}$ conversion. Strikingly, the inclusion of TBAB induces a marked attenuation of the EPR signals under CO_2 atmosphere upon light irradiation, indicating efficient electron transfer from photoexcited Ce-UiO-66-H to CO_2 assisted by TBAB. These findings establish that TBAB promotes photoelectron shuttling from Ce-MOFs to CO_2, thereby enabling the generation of $CO_2^{\bullet-}$ intermediate.

Theoretical calculations further elucidate the electron distribution and energetics following charge transfer. As summarized in Table S9, the $[Br^-\cdots TBA^+]\sim CO_2$ complex exhibits a markedly enhanced electron affinity (−0.88 eV), compared with isolated individual CO_2 (0.41 eV) and TBAB (0.016 eV), indicating that the superior electron-accepting ability of the former. In contrast to the thermodynamically endothermic direct CO_2 to $CO_2^{\bullet-}$ reduction (energy change: 0.66 eV), TBAB facilitates spontaneous adsorption of CO_2 with an adsorption energy of −0.12 eV, forming the $[Br^-\cdots TBA^+]\sim CO_2$ adduct, which exhibits thermodynamically favorable energy change of −0.90 eV upon electron acquisition (Figure 3d). Consistent with EPR and DRIFTS observations, distribution of electron density calculation reveals that the additional electron in the $[Br^-\cdots TBA^+]\sim CO_2$ adduct is mainly localized on the CO_2 moiety, resulting in the production of $CO_2^{\bullet-}$. Moreover, upon electron uptake, the CO_2 molecule undergoes significant structural distortion, with the O=C=O bond angle decreasing from 180° to 133°, giving rise to effective CO_2 activation (Figure 3e).

On the basis of the combined experimental and theoretical evidences, a mechanistic pathway for photocatalytic CO_2 cycloaddition over Ce-UiO-66-X is proposed (Figure 4). Light irradiation initiates the photoexcitation of organic linkers in Ce-MOFs, triggering the LMCT process that efficiently relocates electrons to Ce-oxo nodes. Diverging from conventional direct CO_2-to-$CO_2^{\bullet-}$ mechanism, the $[Br^-\cdots TBA^+]\sim CO_2$ adduct serves as the real electron acceptor, capturing photoinduced electrons from Ce-oxo nodes to generate $[Br^-\cdots TBA^+]\sim CO_2^{\bullet-}$ intermediate. Concurrently, the liberated Br^- facilitates epoxide ring-opening, enabling the nucleophilic $[Br^-\cdots TBA^+]\sim CO_2^{\bullet-}$ species to attack the electrophilic carbon center of the activated epoxide. Subsequent intramolecular cyclization closes the catalytic cycle, yielding cyclic carbonates while regenerating the catalyst and Br^- species.

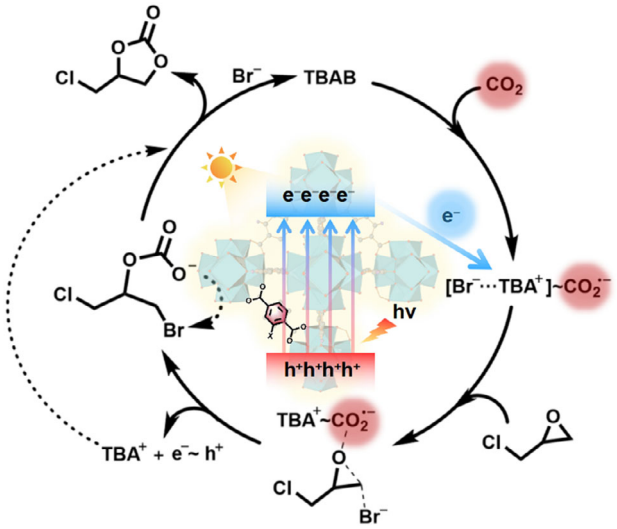

Figure 4. Proposed mechanism for photocatalytic CO_2 cycloaddition over Ce-UiO-66-X (X = Me, H, and F).

Conclusion

In this work, a series of reticular Ce-UiO-66-X photocatalysts with precisely tuned defect densities through linker functionalization have been fabricated. Comprehensive analyses reveal a positive correlation between the electron-withdrawing strength of linker substituents and defect density, following the trend Ce-UiO-66-F > Ce-UiO-66-H > Ce-UiO-66-Me. The photocatalytic CO_2 cycloaddition efficiency is dictated by the interplay between the intrinsic linker absorption energy (ΔE_{abs}) and the defect-regulated charge-transfer barrier (ΔE_{LMCT}). Ce-UiO-66-H achieves an optimal balance between these two parameters, delivering the highest catalytic activity. Significantly, this work unveils the dual and previously unrecognized role of TBAB, where TBA^+ enhances CO_2 affinity while Br^- acts as a nucleophile for epoxide ring-opening. This cooperative effect enables the formation of a $[Br^-\cdots TBA^+]\sim CO_2$ complex that lowers the thermodynamic energy requirement for electron transfer from Ce-MOFs to CO_2. Theoretical calculations further confirm that the $CO_2^{\bullet-}$ species generated via the $[Br^-\cdots TBA^+]\sim CO_2$ adduct requires the thermal energy change of −0.90 eV, which is significantly lower than that of the direct CO_2-to-$CO_2^{\bullet-}$ pathway (0.66 eV), providing the kinetic basis for enhanced photocatalytic CO_2 cycloaddition efficiency. This discovery of the organic amine cation-assisted mechanism for CO_2 activation establishes a new route toward overcoming thermodynamic constraints in light-driven CO_2 valorization.

Acknowledgements

This work is supported by Strategic Priority Research Program of the Chinese Academy of Sciences (XDB0540000, XDB1500203), the National Natural Science Foundation of China (22331009, U22A20401, W2512006, 22101288, 22405258, and 22575260), the Science and Technology Innovation 2025 Program in Ningbo (2022Z205), the Ningbo Yongjiang Talent Introduction Programme (2021A-036-B), Zhejiang Provincial Natural Science Foundation (LQK26E020002), Ningbo Natural Science Foundation (2024J010), the 3315 Program of Ningbo (2020A-32-C), Youth Innovation Promotion Association, Chinese Academy of Sciences, the Foundation of State Key Laboratory of Coal

© 2025 Wiley-VCH GmbH

15213773, 2026, 7, Downloaded from https://onlinelibrary.wiley.com/doi/10.1002/anie.202525369 by University Of Science, Wiley Online Library on [23/02/2026]. See the Terms and Conditions (https://onlinelibrary.wiley.com/terms-and-conditions) on Wiley Online Library for rules of use; OA articles are governed by the applicable Creative Commons License

Conversion (J25-26-610), the Natural Science Foundation Youth Project of Anhui Province (2408085QB070), the China Postdoctoral Science Foundation (2024M753086) and the Fundamental Research Funds for the Central Universities (WK9990250187).

Conflict of Interests

The authors declare no conflict of interest.

Data Availability Statement

The data that support the findings of this study are available from the corresponding author upon reasonable request.

Keywords: CO_2 cycloaddition · Defect engineering · Metal-organic framework · Photocatalysis · TBAB

[1] M. Ding, R. W. Flaig, H.-L. Jiang, O. M. Yaghi, *Chem. Soc. Rev.* **2019**, *48*, 2783–2828, https://doi.org/10.1039/C8CS00829A.
[2] J. Artz, T. E. Müller, K. Thenert, J. Kleinekorte, R. Meys, A. Sternberg, A. Bardow, W. Leitner, *Chem. Rev.* **2018**, *118*, 434–504, https://doi.org/10.1021/acs.chemrev.7b00435.
[3] Z. Liu, K. Wang, Y. Chen, T. Tan, J. Nielsen, *Nat. Catal.* **2020**, *3*, 274–288, https://doi.org/10.1038/s41929-019-0421-5.
[4] A. Allangawi, X. T. Xiao, X. Ma, M. Alsuhami, M. A. Khan, R. Aleisa, Y. Kobayashi, W.-L. Li, M. Rueping, J. Gascon, H. Zhang, *Angew. Chem., Int. Ed.* **2025**, *64*, e202517916.
[5] J. Wu, Y. Li, M. Hu, T. Li, M. Yi, X. Xiao, H. Li, Y. Guo, Y. Kobayashi, M. Rueping, W.-L. Li, H. Zhang, K.-W. Huang, *Angew. Chem., Int. Ed.* **2025**, *64*, e202516163.
[6] S. Huang, B. Yan, S. Wang, X. Ma, *Chem. Soc. Rev.* **2015**, *44*, 3079–3116, https://doi.org/10.1039/C4CS00374H.
[7] Y. Ou, B. Zhang, R. Zhan, S. Liu, W. Wang, S. Tu, Y. Hu, Z. Chen, X. Duan, X. Wang, L. Wang, Y. Sun, *Nat. Commun.* **2025**, *16*, 7956. https://doi.org/10.1038/s41467-025-63257-w.
[8] D. Lee, S. Sun, J. Kwon, H. Park, M. Jang, E. Park, B. Son, Y. Jung, T. Song, U. Paik, *Adv. Mater.* **2020**, *32*, 1905573, https://doi.org/10.1002/adma.201905573.
[9] C. Qiao, W. Shi, A. Brandolese, J. Benet-Buchholz, E. C. Escudero-Adán, A. W. Kleij, *Angew. Chem., Int. Ed.* **2022**, *61*, e202205053, https://doi.org/10.1002/anie.202205053.
[10] P. Wu, Y. Li, J.-J. Zheng, N. Hosono, K.-I. Otake, J. Wang, Y. Liu, L. Xia, M. Jiang, S. Sakaki, S. Kitagawa, *Nat. Commun.* **2019**, *10*, 4362. https://doi.org/10.1038/s41467-019-12414-z.
[11] C. Maeda, T. Taniguchi, K. Ogawa, T. Ema, *Angew. Chem., Int. Ed.* **2015**, *54*, 134–138, https://doi.org/10.1002/anie.201409729.
[12] L. Liang, C. Liu, F. Jiang, Q. Chen, L. Zhang, H. Xue, H.-L. Jiang, J. Qian, D. Yuan, M. Hong, *Nat. Commun.* **2017**, *8*, 1233. https://doi.org/10.1038/s41467-017-01166-3.
[13] M. K. Dinker, M.-M. Li, K. Zhao, M. Zuo, L. Ding, X.-Q. Liu, L.-B. Sun, *Angew. Chem., Int. Ed.* **2023**, *62*, e202306495.
[14] Y. Wang, H. Liu, Q. Shi, Z. Miao, H. Duan, Y. Wang, H. Rong, J. Zhang, *Angew. Chem., Int. Ed.* **2024**, *63*, e202404911, https://doi.org/10.1002/anie.202404911.
[15] S.-C. Fan, J.-W. Wang, W. Yuan, P. Zhang, Y. Wang, Q.-G. Zhai, *Chem* **2024**, *10*, 1804–1820, https://doi.org/10.1016/j.chempr.2024.01.031.
[16] P. K. Prajapati, A. Kumar, S. L. Jain, *ACS Sustainable Chem. Eng.* **2018**, *6*, 7799–7809, https://doi.org/10.1021/acssuschemeng.8b00755.
[17] N. Saini, A. Malik, S. L. Jain, *Coord. Chem. Rev.* **2024**, *502*, 215636, https://doi.org/10.1016/j.ccr.2023.215636.
[18] M. Mikkelsen, M. Jørgensen, F. C. Krebs, *Energy Environ. Sci.* **2010**, *3*, 43–81, https://doi.org/10.1039/B912904A.
[19] Y.-T. Zheng, S. Li, N.-Y. Huang, X. Li, Q. Xu, *Coord. Chem. Rev.* **2024**, *510*, 215858, https://doi.org/10.1016/j.ccr.2024.215858.
[20] C. Feng, M. Hu, S. Zuo, J. Luo, P. Castaño, Y. Ren, M. Rueping, H. Zhang, *Adv. Mater.* **2025**, *37*, 2411813, https://doi.org/10.1002/adma.202411813.
[21] M. North, R. Pasquale, *Angew. Chem., Int. Ed.* **2009**, *48*, 2946–2948, https://doi.org/10.1002/anie.200805451.
[22] C. Huang, J. Dong, W. Sun, Z. Xue, J. Ma, L. Zheng, C. Liu, X. Li, K. Zhou, X. Qiao, Q. Song, W. Ma, L. Zhang, Z. Lin, T. Wang, *Nat. Commun.* **2019**, *10*, 2779. https://doi.org/10.1038/s41467-019-10547-9.
[23] G. Ji, Z. Yang, H. Zhang, Y. Zhao, B. Yu, Z. Ma, Z. Liu, *Angew. Chem., Int. Ed.* **2016**, *55*, 9685–9689, https://doi.org/10.1002/anie.201602667.
[24] B. A. Rosen, A. Salehi-Khojin, M. R. Thorson, W. Zhu, D. T. Whipple, P. J. Kenis, R. I. Masel, *Science* **2011**, *334*, 643–644, https://doi.org/10.1126/science.1209786.
[25] J.-M. McGregor, J. T. Bender, A. S. Petersen, L. Cañada, J. Rossmeisl, J. F. Brennecke, J. Resasco, *Nat. Catal.* **2025**, *8*, 79–91, https://doi.org/10.1038/s41929-024-01278-2.
[26] Y. Liu, J. Sun, H. Huang, L. Bai, X. Zhao, B. Qu, L. Xiong, F. Bai, J. Tang, L. Jing, *Nat. Commun.* **2023**, *14*, 1457. https://doi.org/10.1038/s41467-023-36980-5.
[27] D. Yang, Q. Zhu, B. Han, *The Innovation* **2020**, *1*, 10016.
[28] H. Furukawa, K. E. Cordova, M. O'Keeffe, O. M. Yaghi, *Science* **2013**, *341*, 1230444, https://doi.org/10.1126/science.1230444.
[29] B.-N. T. Nguyen, T. T. Y. Tan, K.-I. Otake, S. Kitagawa, J. Y. C. Lim, *Angew. Chem., Int. Ed.* **2025**, *64*, e202504017.
[30] Y. Chen, H. Xie, Y. Zhong, F. Sha, K. O. Kirlikovali, X. Wang, C. Zhang, Z. Li, O. K. Farha, *J. Am. Chem. Soc.* **2024**, *146*, 11202–11210.
[31] H.-C. J. Zhou, S. Kitagawa, *Chem. Soc. Rev.* **2014**, *43*, 5415–5418, https://doi.org/10.1039/C4CS90059F.
[32] A. Ebadi Amooghin, H. Sanaeepur, R. Luque, H. Garcia, B. Chen, *Chem. Soc. Rev.* **2022**, *51*, 7427–7508, https://doi.org/10.1039/D2CS00442A.
[33] X. Zhao, Y. Wang, D.-S. Li, X. Bu, P. Feng, *Adv. Mater.* **2018**, *30*, 1705189, https://doi.org/10.1002/adma.201705189.
[34] F.-A. Guo, J. Wang, C. Chen, X. Dong, X. Li, H. Wang, P. Guo, Y. Han, J. Li, *Angew. Chem., Int. Ed.* **2023**, *62*, e202303527, https://doi.org/10.1002/anie.202303527.
[35] G. S. G. Farmer, D. J. Cheney, K.-N. Truong, N. Gedikoglu, B. P. Mali, D. Markad, D. Antypov, F. Blanc, A. P. Katsoulidis, M. J. Rosseinsky, *J. Am. Chem. Soc.* **2025**, *147*, 27586–27598, https://doi.org/10.1021/jacs.5c05854.
[36] Y. Qin, Z. Li, Y. Duan, J. Guo, M. Zhao, Z. Tang, *Matter* **2022**, *5*, 3260–3310.
[37] P. M. Stanley, J. Haimerl, C. Thomas, A. Urstoeger, M. Schuster, N. B. Shustova, A. Casini, B. Rieger, J. Warnan, R. A. Fischer, *Angew. Chem., Int. Ed.* **2021**, *60*, 17854–17860, https://doi.org/10.1002/anie.202102729.
[38] H. Zhang, J. Wei, J. Dong, G. Liu, L. Shi, P. An, G. Zhao, J. Kong, X. Wang, X. Meng, J. Zhang, J. Ye, *Angew. Chem., Int. Ed.* **2016**, *55*, 14310–14314, https://doi.org/10.1002/anie.201608597.
[39] R. Xu, D.-H. Si, S.-S. Zhao, Q.-J. Wu, X.-S. Wang, T.-F. Liu, H. Zhao, R. Cao, Y.-B. Huang, *J. Am. Chem. Soc.* **2023**, *145*, 8261–8270, https://doi.org/10.1021/jacs.3c02370.
[40] Y. Wang, J.-X. Wei, H.-L. Tang, L.-H. Shao, L.-Z. Dong, X.-Y. Chu, Y.-X. Jiang, G.-L. Zhang, F.-M. Zhang, Y.-Q. Lan,

© 2025 Wiley-VCH GmbH

15213773, 2026, 7, Downloaded from https://onlinelibrary.wiley.com/doi/10.1002/anie.202525369 by University Of Science, Wiley Online Library on [23/02/2026]. See the Terms and Conditions (https://onlinelibrary.wiley.com/terms-and-conditions) on Wiley Online Library for rules of use; OA articles are governed by the applicable Creative Commons License

Nat. Commun. **2024**, *15*, 8818. https://doi.org/10.1038/s41467-024-53066-y.
[41] Q. Yang, H. Liu, Y. Lin, D. Su, Y. Tang, L. Chen, *Adv. Mater.* **2024**, *36*, 2310912, https://doi.org/10.1002/adma.202310912.
[42] K. Sun, Y. Qian, D. Li, H.-L. Jiang, *Adv. Mater.* **2024**, 2411118, https://doi.org/10.1002/adma.202411118.
[43] X.-P. Wu, L. Gagliardi, D. G. Truhlar, *J. Am. Chem. Soc.* **2018**, *140*, 7904–7912, https://doi.org/10.1021/jacs.8b03613.
[44] X.-P. Wu, L. Gagliardi, D. G. Truhlar, *J. Chem. Phys.* **2019**, *150*, 041701–041711, https://doi.org/10.1063/1.5043538.
[45] G. B. Panetti, D.-C. Sergentu, M. R. Gau, P. J. Carroll, J. Autschbach, P. J. Walsh, E. J. Schelter, *Nat. Commun.* **2021**, *12*, 1713. https://doi.org/10.1038/s41467-021-21766-4.
[46] K. Sun, Y. Qian, H.-L. Jiang, *Angew. Chem., Int. Ed.* **2023**, *62*, e202217565.
[47] Q. Yang, Y. Wang, X. Tang, Q. Zhang, S. Dai, H. Peng, Y. Lin, Z. Tian, Z. Lu, L. Chen, *Nano Lett.* **2022**, *22*, 838–845, https://doi.org/10.1021/acs.nanolett.1c04574.
[48] S.-Q. Wang, X. Gu, X. Wang, X.-Y. Zhang, X.-Y. Dao, X.-M. Cheng, J. Ma, W.-Y. Sun, *Chem. Eng. J.* **2022**, *429*, 132157, https://doi.org/10.1016/j.cej.2021.132157.
[49] A. D. Vos, K. Hendrickx, P. V. D. Voort, V. V. Speybroeck, K. Lejaeghere, *Chem. Mater.* **2017**, *29*, 3006–3019, https://doi.org/10.1021/acs.chemmater.6b05444.
[50] H. Liu, M. Cheng, Y. Liu, G. Zhang, L. Li, L. Du, B. Li, S. Xiao, G. Wang, X. Yang, *Coordin. Chem. Rev.* **2022**, *458*, 214428, https://doi.org/10.1016/j.ccr.2022.214428.
[51] B. Liu, C. Li, G. Zhang, X. Yao, S. S. C. Chuang, Z. Li, *ACS Catal.* **2018**, *8*, 10446–10456, https://doi.org/10.1021/acscatal.8b00415.
[52] Y.-Z. Chen, B. Gu, T. Uchida, J. Liu, X. Liu, B.-J. Ye, Q. Xu, H.-L. Jiang, *Nat. Commun.* **2019**, *10*, 3462–3472, https://doi.org/10.1038/s41467-019-11449-6.
[53] X. Jiang, Y. Zhang, J. Jiang, Y. Rong, Y. Wang, Y. Wu, C. Pan, *J. Phys. Chem. C* **2012**, *116*, 22619–22624, https://doi.org/10.1021/jp307573c.
[54] H. Wu, Y. S. Chua, V. Krungleviciute, M. Tyagi, P. Chen, T. Yildirim, W. Zhou, *J. Am. Chem. Soc.* **2013**, *135*, 10525–10532, https://doi.org/10.1021/ja404514r.
[55] S. Yuan, L. Zou, J.-S. Qin, J. Li, L. Huang, L. Feng, X. Wang, M. Bosch, A. Alsalme, T. Cagin, H.-C. Zhou, *Nat. Commun.* **2017**, *8*, 15356, https://doi.org/10.1038/ncomms15356.
[56] S. Dai, C. Simms, G. Patriarche, M. Daturi, A. Tissot, T. N. Parac-Vogt, C. Serre, *Nat. Commun.* **2024**, *15*, 3434. https://doi.org/10.1038/s41467-024-47426-x.
[57] P. Ji, T. Drake, A. Murakami, P. Oliveres, J. H. Skone, W. Lin, *J. Am. Chem. Soc.* **2018**, *140*, 10553–10561, https://doi.org/10.1021/jacs.8b05765.
[58] G. C. Shearer, S. Chavan, S. Bordiga, S. Svelle, U. Olsbye, K. P. Lillerud, *Chem. Mater.* **2016**, *28*, 3749–3761, https://doi.org/10.1021/acs.chemmater.6b00602.
[59] S. Rojas-Buzo, B. Bohigues, D. Salusso, A. Corma, M. Moliner, S. Bordiga, *ACS Catal.* **2023**, *13*, 9171–9180, https://doi.org/10.1021/acscatal.3c00502.
[60] R. Huang, J. Rintjema, J. González-Fabra, E. Martín, E. C. Escudero-Adán, C. Bo, A. Urakawa, A. W. Kleij, *Nat. Catal.* **2019**, *2*, 62–70.
[61] Y. Wang, S. Tang, G. Yang, S. Wang, D. Ma, Y. Qiu, *Angew. Chem., Int. Ed.* **2022**, *61*, e202207746, https://doi.org/10.1002/anie.202207746.
[62] C. Huang, W. Ma, X. Zheng, M. Xu, X. Qi, Q. Lu, *J. Am. Chem. Soc.* **2022**, *144*, 1389–1395.
[63] H. Wang, Q. Tang, Z. Wu, *ACS Sustainable Chem. Eng.* **2021**, *9*, 8425–8434, https://doi.org/10.1021/acssuschemeng.1c01155.
[64] G. Zhai, Y. Liu, Y. Mao, H. Zhang, L. Lin, Y. Li, Z. Wang, H. Cheng, P. Wang, Z. Zheng, Y. Dai, B. Huang, *Appl. Catal. B Environ.* **2022**, *301*, 120793, https://doi.org/10.1016/j.apcatb.2021.120793.
[65] E. Abi-Aad, A. Bennani, J.-P. Bonnelle, A. Aboukaïs, *J. Chem. Soc., Faraday Trans.* **1995**, *91*, 99–104, https://doi.org/10.1039/FT9959100099.

Manuscript received: November 17, 2025
Revised manuscript received: December 12, 2025
Manuscript accepted: December 23, 2025
Version of record online: December 31, 2025

© 2025 Wiley-VCH GmbH

15213773, 2026, 7, Downloaded from https://onlinelibrary.wiley.com/doi/10.1002/anie.202525369 by University Of Science, Wiley Online Library on [23/02/2026]. See the Terms and Conditions (https://onlinelibrary.wiley.com/terms-and-conditions) on Wiley Online Library for rules of use; OA articles are governed by the applicable Creative Commons License